Eurographics/ IEEE-VGTC Symposium on Visualization (2006)
Thomas Ertl, Ken Joy, and Beatriz Santos (Editors)

Path Line Oriented Topology for Periodic 2D Time-Dependent Vector Fields

K. Shi[1], H. Theisel[1], T. Weinkauf[2], H. Hauser[3], H.-C. Hege[2] and H.-P. Seidel[1]

[1] MPI Informatik, Saarbrücken, Germany — {skyshi, theisel, hpseidel}@mpi-inf.mpg.de
[2] Zuse Institute Berlin (ZIB), Berlin, Germany — {weinkauf, hege}@zib.de
[3] VRVis Vienna, Austria — hauser@vrvis.at

Abstract

This paper presents an approach to extracting a path line oriented topological segmentation for periodic 2D time-dependent vector fields. Topological methods aiming in capturing the asymptotic behavior of path lines rarely exist because path lines are usually only defined over a fixed time-interval, making statements about their asymptotic behavior impossible. For the data class of periodic vector fields, this restriction does not apply any more. Our approach detects critical path lines as well as basins from which the path lines converge to the critical ones. We demonstrate our approach on a number of test data sets.

Categories and Subject Descriptors (according to ACM CCS): I.3.3 [Computer Graphics]: Line and Curve Generation I.3.3 [Computer Graphics]: Picture/Image Generation I.3.7 [Computer Graphics]: Three-Dimensional Graphics and Realism

1. Introduction

Over the last decade, topological methods have become a standard tool in vector field visualization. Initially introduced as a visualization tool in [HH89], topological methods have been extended to higher order critical points [SKMR98], boundary switch points [dLvL99a], and closed separatrices [WS01]. In addition, topological methods have been applied to simplify [dLvL99a, dLvL99b, TSH00, TSH01, WTS*05], smooth [WJE01], compress [LRR00, TRS03] and construct [The02, WTHS04b] vector fields. The topology of 3D vector fields is visualized in [GLL91, LDG98, MBS*04, TWHS03, WTHS04a].

The main idea behind topological methods is to segment a vector field into areas of similar asymptotic behavior. This means to classify each point $\mathbf{x}$ in the domain with respect to the asymptotic behavior of the characteristic curve through it, i.e., a forward and backward integration starting from $\mathbf{x}$ with an integration time converging to infinity is considered. Usually, this integration does not have to be carried out for every point but only for a certain number of starting points of separatrices.

For time-dependent vector fields there exists a number of relevant characteristic curves, such as stream lines, path lines, streak lines and time lines. Among them, stream lines and path lines have the uniqueness property: through each point in the space-time domain there is exactly one stream line and one path line passing through. This gives that two different kinds of topologies can be considered: a stream line oriented topology segmenting areas of similar stream line behavior, and a path line oriented topology which does so for path lines. Extracting a stream line oriented topology ends up in tracking critical points and considering certain bifurcations. A number of approaches for this exist [TWSH02, WSH01, TS03, GTS04, TWHS05].

Path lines are important structures in time-dependent vector fields because they describe the path of massless particles in a flow. Hence, a path line oriented segmentation gives a different kind of insight into the vector field data than the stream lines. Unfortunately, path line oriented topological methods rarely exist because a strong restriction applies: since path lines move constantly forward in time and real life data sets are usually given only in a fixed time interval, a path line integration until infinity cannot be carried out: the integration stops when the maximal time of the given data set is

reached. Therefore, a topological segmentation based on the asymptotic behavior of path lines usually does not exist. One approach to avoid this problem was presented in [TWHS05]. There, instead of an asymptotic behavior of path lines, only their local behavior was considered for segmentation. This segmentation delivers regions of locally attracting, repelling or saddle-like behavior of the path lines. However, it is not a topological one in the classical sense because it does not incorporate any asymptotic behavior of the path lines.

This paper presents the (to the best of our knowledge) first approach to topologically analyzing and visualizing the asymptotic behavior of path lines. We achieve this by restricting ourselves to *periodic* time-dependent vector fields. We think that this class of vector fields deserves special consideration since many numerical flow simulations are actually periodic (or pseudo-periodic) flows. Examples of the visual analysis of periodic flow fields (but not a topological analysis of path lines) can be found in [TWHS05, TSW*05].

For periodic vector fields, the time-domain is not restricted to a certain interval but can be extended to any time by periodically repeating the given field. Hence, an analysis of the asymptotic behavior of path lines becomes possible.

The rest of the paper is organized as follows: section 2 recalls the concepts of stream line and path line oriented topology and gives a setup to distinguish and analyze them. Section 3 analyzes the behavior of path lines of periodic vector fields and shows that their asymptotic behavior can be obtained by a topological segmentation of a 2D Poincaré map. Section 4 describes how to achieve this segmentation: section 4.1 classifies critical points in a Poincaré map, while section 4.2 explains how to get the sectors of different asymptotic behavior. Section 5 describes our algorithm to extracting the topological skeleton. Section 6 shows a number of applications of our approach, while conclusions are drawn in section 7.

2. Stream line and path line oriented topology

Given is a 2D time-dependent vector field $\mathbf{v}(\mathbf{x},t)$ in the space-time domain $D \times [t_{min}, t_{max}]$ where (for the sake of simplicity) $D = [x_{min}, x_{max}] \times [y_{min}, y_{max}]$. Then $\mathbf{x}$ describes the spatial domain and t is the temporal component. In order to distinguish stream lines and path lines, we derive two 3D vector fields $\mathbf{s}$ and $\mathbf{p}$ by adding a constant component to $\mathbf{v}$ (see also [TWHS05]):

$$\mathbf{s}(\mathbf{x},t) = \begin{pmatrix} \mathbf{v}(\mathbf{x},t) \\ 0 \end{pmatrix} \quad , \quad \mathbf{p}(\mathbf{x},t) = \begin{pmatrix} \mathbf{v}(\mathbf{x},t) \\ 1 \end{pmatrix}. \qquad (1)$$

This way the stream lines of $\mathbf{s}$ correspond to the stream lines of $\mathbf{v}$, while the stream lines of $\mathbf{p}$ correspond to the path lines of $\mathbf{v}$. Therefore, a path line oriented topological segmentation of $\mathbf{v}$ corresponds to a segmentation of the stream lines of $\mathbf{p}$. Unfortunately, such a segmentation of $\mathbf{p}$ cannot be made by applying conventional topological methods of 3D vector fields because an asymptotic analysis of a stream line in $\mathbf{p}$ is impossible: every stream line integration in $\mathbf{p}$ is guaranteed to leave the domain $D \times [t_{min}, t_{min}]$ after a while, making it impossible to consider the asymptotic behavior. This restriction does not hold any more when moving forward to periodic vector fields.

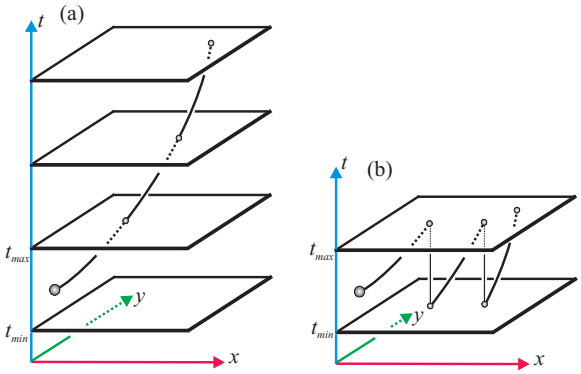

Figure 1: *Two equivalent approaches of a stream line integration in a periodic field* $\mathbf{p}$*: (a) In the unbounded time-domain; (b) Periodically continued in the time-domain* $[t_{min}, t_{max}]$.

3. Periodic vector fields

If $\mathbf{v}$ is a periodic-in-time vector field, it is sufficient to consider one period which can be repeated as often as necessary. We assume that $\mathbf{v}$ describes one period, which means that $\mathbf{v}(\mathbf{x}, t_{min}) = \mathbf{v}(\mathbf{x}, t_{max})$. Then we can assume $\mathbf{v}$ to be defined in the whole domain $D \times \mathbb{R}$ by setting

$$\mathbf{v}(\mathbf{x},t) = \mathbf{v}(\mathbf{x},\ t + k\,\Delta t)$$

where $\Delta t = (t_{max} - t_{min})$ and k is an integer chosen such that $t_{min} \leq t + k\,\Delta t < t_{max}$. In a similar way, $\mathbf{p}$ is defined over $D \times \mathbb{R}$.

In order to integrate a stream line in the periodic field $\mathbf{p}$ (which corresponds to a path line of $\mathbf{v}$), two equivalent strategies can be applied:

- The integration is done over the unbounded time-domain as illustrated in figure 1a.
- If the integration approaches a point $(\mathbf{x}, t_{max})$, it is mapped to $(\mathbf{x}, t_{min})$. From there, the integration is continued until t_{max} is reached again. Figure 1b illustrates this.

Note that in all figures throughout this paper the coordinate system is shown as follows: red/green coordinate axes denote the (x, y)- domain, the blue axis shows the time component.

Our approach to do a topological segmentation of path lines starts with picking a certain reference time τ with $t_{min} \leq \tau < t_{max}$. We aim at a segmentation of the asymptotic behavior of all path lines starting at the time τ. To do so, two

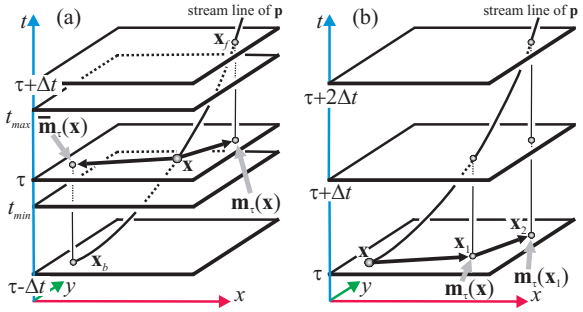

Figure 2: *(a) The definition of* $\mathbf{m}_\tau(\mathbf{x})$ *and* $\bar{\mathbf{m}}_\tau(\mathbf{x})$*; (b) A continuous forward integration of* $\mathbf{p}$ *corresponds to a discrete integration of* $\mathbf{m}_\tau(\mathbf{x})$.

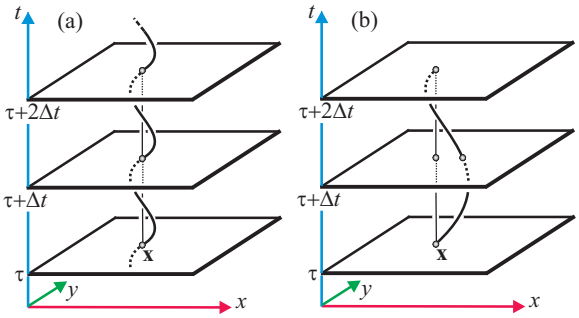

Figure 3: *(a) A critical path line corresponds to fix points in* $\mathbf{m}_\tau$, $\bar{\mathbf{m}}_\tau$. *(b) Critical path line over two time periods.*

2D maps $\mathbf{m}_\tau(\mathbf{x})$ and $\bar{\mathbf{m}}_\tau(\mathbf{x})$ are constructed. For $\mathbf{m}_\tau(\mathbf{x})$, we start a forward integration of $\mathbf{p}$ from $(\mathbf{x},\tau)$ until one of the following cases occurs:

1. The integration reaches the time level $\tau+\Delta t$, i.e. comes to a certain point $(\mathbf{x}_f,\tau+\Delta t)$. Then we set $\mathbf{m}_\tau(\mathbf{x})=\mathbf{x}_f$.
2. The integration leaves D before reaching the level $\tau+\Delta t$. In this case we mark $\mathbf{m}_\tau(\mathbf{x})$ as undefined.

In a similar way we compute $\bar{\mathbf{m}}_\tau(\mathbf{x})$ by starting a backward integration of $\mathbf{p}$ from $(\mathbf{x},\tau)$ until the time level $\tau-\Delta t$ is reached at a point $(\mathbf{x}_b,\tau-\Delta t)$, or until the integration leaves D. In the first case, we set $\bar{\mathbf{m}}_\tau(\mathbf{x})=\mathbf{x}_b$, in the second case $\bar{\mathbf{m}}_\tau(\mathbf{x})$ is undefined. Figure 2a illustrates the definition of $\mathbf{m}_\tau(\mathbf{x})$ and $\bar{\mathbf{m}}_\tau(\mathbf{x})$.

Instead of the definition of the maps $\mathbf{m}_\tau(\mathbf{x})$ and $\bar{\mathbf{m}}_\tau(\mathbf{x})$ described above, we can also use a vector-oriented description of the map:

$$\mathbf{q}_\tau(\mathbf{x})=\mathbf{m}_\tau(\mathbf{x})-\mathbf{x} \quad , \quad \bar{\mathbf{q}}_\tau(\mathbf{x})=\bar{\mathbf{m}}_\tau(\mathbf{x})-\mathbf{x} \tag{2}$$

Since $\mathbf{m}_\tau(\mathbf{x})$ and $\mathbf{q}_\tau(\mathbf{x})$ can be easily transformed into each other, we will switch between both formulations in order to simplify the notation of our approach. Note that in general $\bar{\mathbf{q}}_\tau \neq -\mathbf{q}_\tau$.

The maps $\mathbf{m}_\tau$ and $\bar{\mathbf{m}}_\tau$ can be interpreted as 2D Poincaré maps [LKG98]. In order to analyze the asymptotic behavior of a path line starting from $(\mathbf{x},\tau)$ in forward direction, we do not have to integrate $\mathbf{p}$ any more but can restrict ourselves to a sequence of maps of $\mathbf{m}_\tau(\mathbf{x})$:

$$\mathbf{x}_0=\mathbf{x} \quad , \quad \mathbf{x}_{i+1}=\mathbf{m}_\tau(\mathbf{x}_i) \tag{3}$$

and considering the asymptotic behavior for $i\to\infty$. Figure 2b illustrates this. A similar statement holds for the backward integration of $\mathbf{p}$ and a sequence of maps of $\bar{\mathbf{m}}_\tau$. Note that (3) is equivalent to a numerical Euler integration of $\mathbf{q}_\tau$ with the step size 1: $\mathbf{x}_{i+1}=\mathbf{x}_i+1\,\mathbf{q}_\tau(\mathbf{x}_i)$.

Both Poincré maps $\mathbf{m}_\tau$ and $\bar{\mathbf{m}}_\tau$ can be considered as discrete invertible dynamical systems: there are no two distinct points which are mapped to the same point by $\mathbf{m}_\tau$ or $\bar{\mathbf{m}}_\tau$. In other words: $\mathbf{m}_\tau$ and $\bar{\mathbf{m}}_\tau$ are inverse to each other:

$$\bar{\mathbf{m}}_\tau(\mathbf{m}_\tau(\mathbf{x}))=\mathbf{m}_\tau(\bar{\mathbf{m}}_\tau(\mathbf{x}))=\mathbf{x} \tag{4}$$

for every $\mathbf{x}$ where both $\mathbf{m}_\tau$ and $\bar{\mathbf{m}}_\tau$ are defined.

A special role in the further analysis of the path lines play isolated fix points of $\mathbf{m}_\tau$ and $\bar{\mathbf{m}}_\tau$, i.e., points $\mathbf{x}$ with $\mathbf{m}_\tau(\mathbf{x})=\bar{\mathbf{m}}_\tau(\mathbf{x})=\mathbf{x}$. (This is equivalent to critical points in $\mathbf{q}_\tau$, $\bar{\mathbf{q}}_\tau$.) The fix points of $\mathbf{m}_\tau$ and $\bar{\mathbf{m}}_\tau$ correspond to certain path lines which we call *critical path lines* because they have a well-defined asymptotic behavior: they repeat the same spatial cycle in every time period. Figure 3a gives an illustration.

The critical path lines will be the basis of our topological segmentation: we classify path lines whether they converge to a critical path line in forward or backward integration respectively. Similar to critical points of a vector field, critical path lines can act as sources, sinks, or saddles.

Note that more critical path lines may occur when considering two or more time periods. Such a critical path line over n time periods corresponds to a fix point of the map $\mathbf{m}_\tau{}^n$. Figure 3b illustrates an example for $n=2$. However, in our applications we only considered simple (one period) critical path lines.

4. Topological segmentation of 2D Poincaré maps

The segmentation of areas of similar path line behavior corresponds to the topological segmentation of the 2D Poincaré maps $\mathbf{m}_\tau$ and $\bar{\mathbf{m}}_\tau$ respectively. Critical path lines in $\mathbf{p}$ correspond to fix points in $\mathbf{m}_\tau$ and $\bar{\mathbf{m}}_\tau$. They may act as sources, sinks or saddle path lines building α- and ω-basins in D. In this section we show how to find this segmentation by a topological analysis of $\mathbf{m}_\tau$ and $\bar{\mathbf{m}}_\tau$. Since $\mathbf{m}_\tau$ and $\bar{\mathbf{m}}_\tau$ can be considered as discrete dynamical systems, classical topological vector field approaches fail to give the correct segmentation because they reflect continuous dynamical systems. In particular, the following points apply:

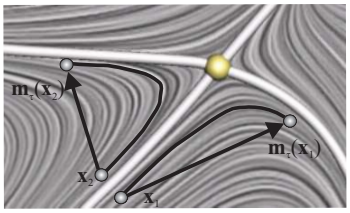

Figure 4: *Pseudo discontinuities in $\mathbf{m}_\tau$: if $\mathbf{x}_1$ and $\mathbf{x}_2$ are close but at different sides of a separatrix of $\mathbf{v}(\mathbf{x}) = \mathbf{v}(\mathbf{x},t)$, $\mathbf{m}_\tau$ has too large changes that it is impossible for discrete numerical method to deal with it though it is still continuous.*

1. Although $\mathbf{p}$ is continuous, both $\mathbf{m}_\tau$ and $\bar{\mathbf{m}}_\tau$ may have pseudo discontinuities. It means that $\mathbf{m}_\tau$ and $\bar{\mathbf{m}}_\tau$ are still continuous mathematically, but they may have areas with tremendous large gradient, which appear as discontinuities for discrete treatment.
2. The classification of the fix points of $\mathbf{m}_\tau$ and $\bar{\mathbf{m}}_\tau$ in sources, sinks and saddles can be obtained by an eigenanalysis of the Jabobians of $\mathbf{m}_\tau$ and $\bar{\mathbf{m}}_\tau$ but differers from the classification for smooth vector fields [Tso92, Löf98].
3. The separating structures of the basins are generally not stream lines of the vector fields $\mathbf{q}_\tau$ and $\bar{\mathbf{q}}_\tau$. Because of this, they can intersect in non-critical points of $\mathbf{q}_\tau$ and $\bar{\mathbf{q}}_\tau$.

To see the first point, we consider the example of a steady 2D vector field $\mathbf{v}(\mathbf{x}) = \mathbf{v}(\mathbf{x},t)$ which can also be considered as as periodic time-depending vector field. Setting a certain time Δt as period, $\mathbf{m}_\tau(\mathbf{x})$ is obtained by a stream line integration of $\mathbf{v}$ at $\mathbf{x}$ over a time Δt. If $\mathbf{v}$ consists of saddles, its separatrices may induce tremendous changes in $\mathbf{m}_\tau$ that it appears as discontinuities for normal discrete numerical programs. Figure 4 illustrates this. The points 2 and 3 are treated in the next subsections.

Critical points of discrete non-invertible dynamical systems and their corresponding basins have been extracted and visualized in [BMH01, HMBG01], ending up in non-connected or even fractal-shaped basins. However, for our purposes the approach simplifies because $\mathbf{m}_\tau$ and $\bar{\mathbf{m}}_\tau$ are invertible.

4.1. Classifying critical points

The classification of a first order critical point in a discrete dynamical system is well-understood [Tso92, Löf98] and differs from the classification of a continuous system. Given a first order approximation of $\mathbf{m}_\tau$

$$\mathbf{m}_\tau(\mathbf{x}) = \mathbf{J}\,\mathbf{x} \tag{5}$$

where $\mathbf{J}$ is the 2×2 Jacobian matrix, $\mathbf{m}_\tau$ has a fix point at $(0,0)$. To capture the asymptotic converging/diverging behavior of the sequence (3) for $i \to \infty$ in a vicinity of $(0,0)$, we consider the eigenvales λ_1, λ_2 and the corresponding

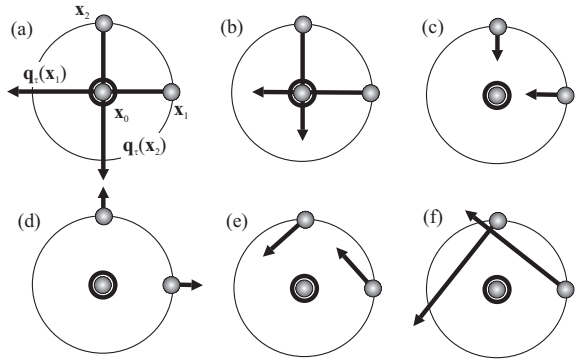

Figure 5: *Classification of sources/sinks of $\mathbf{m}_\tau$: (a) repelling/alternating; (b) attracting/alternating; (c) attracting/non-alternating (d) repelling/non-alternating; (e) attracting/rotating; (f) repelling/rotating.*

eigenvectors $\mathbf{e}_1$, $\mathbf{e}_2$ of $\mathbf{J}$. Based on the eigenvalues, we get the following classification

$$\begin{aligned}
\|\lambda_j\| > 1 &\;\rightarrow\; \text{repelling behavior}\\
\|\lambda_j\| < 1 &\;\rightarrow\; \text{attracting behavior}\\
\mathrm{Im}(\lambda_j) \neq 0 &\;\rightarrow\; \text{rotating behavior}\\
\mathrm{Im}(\lambda_j) = 0\,,\ \mathrm{Re}(\lambda_j) < 0 &\;\rightarrow\; \text{alternating behavior}\\
\mathrm{Im}(\lambda_j) = 0\,,\ \mathrm{Re}(\lambda_j) > 0 &\;\rightarrow\; \text{non-alternating behavior}
\end{aligned}$$

for $j = 1,2$. Figure 5 illustrates some examples of sources and sinks of $\mathbf{m}_\tau$. There, in order to describe the linear approximation $\mathbf{m}_\tau$, we show three points and their assigned vectors $\mathbf{q}_\tau$: the fix point $\mathbf{x}_0$, and two more points $\mathbf{x}_1$, $\mathbf{x}_2$ in the direction of the two eigenvectors of $\mathbf{J}$. The circles around the fix points denote whether the map moves closer or further away from the fix point: if the two arrows of $\mathbf{q}_\tau$ point inside the circle, an attracting behavior of $\mathbf{q}_\tau$ is present.

If $\mathbf{m}_\tau$ is linear as given in (5), then $\bar{\mathbf{m}}_\tau$ is linear as well:

$$\bar{\mathbf{m}}_\tau(\mathbf{x}) = \mathbf{J}^{-1}\,\mathbf{x}. \tag{6}$$

Since the eigenvalues/eigenvectors of $\mathbf{J}^{-1}$ are $1/\lambda_j$, $\mathbf{e}_j$ for $j = 1,2$, there are the following correlations between $\mathbf{m}_\tau$ and $\bar{\mathbf{m}}_\tau$:

behavior of $\mathbf{m}_\tau$	behavior of $\bar{\mathbf{m}}_\tau$
repelling	attracting
attracting	repelling
saddle	saddle
alternating	alternating
non-alternating	non-alternating
rotating	rotating

4.2. Getting the topological sectors

For continuous dynamical systems, the different basins are separated by stream lines starting from saddle points. How-

ever, such a stream line integration does not exist for the discrete systems $\mathbf{m}_\tau$ and $\bar{\mathbf{m}}_\tau$. Therefore we apply a point-wise approach: for every point $\mathbf{x}$ in D, we integrate $\mathbf{m}_\tau$ using (3) until one of the following conditions is fulfilled:

- $\mathbf{x}_i$ comes close to a fix point of $\mathbf{m}_\tau$,
- $\mathbf{x}_i$ leaves the domain D,
- i exceeds a certain threshold of maximal iterations.

In the first case we assume $\mathbf{x}$ to be part of the basin of the fix point. This means that the path line starting at $(\mathbf{x},\tau)$ converges to a critical path line under forward integration. In the second case, the path line is known to leaving the domain under forward integration. In the last case, $\mathbf{x}$ is marked as unknown because we could not get a statement about the asymptotic behavior of the path line starting from $(\mathbf{x},t)$.

5. The algorithm

In this section we formulate our algorithm to get the path line oriented topological segmentation of a periodic 2D vector field $\mathbf{v}(\mathbf{x},t)$:

1. Pick a time τ with $t_{min} \leq \tau < t_{max}$ for which we compute the topological segmentation.
2. Compute the Poincaré maps $\mathbf{m}_\tau$ and $\bar{\mathbf{m}}_\tau$, or equivalently, the vector fields $\mathbf{q}_\tau$ and $\bar{\mathbf{q}}_\tau$.
3. Extract the fix points of $\mathbf{m}_\tau$ and $\bar{\mathbf{m}}_\tau$.
4. Classify the fix points of $\mathbf{m}_\tau$ and $\bar{\mathbf{m}}_\tau$.
5. Assign a unique color to each sink of $\mathbf{m}_\tau$ and $\bar{\mathbf{m}}_\tau$.
6. For each $\mathbf{x} \in D$: repeatedly apply $\mathbf{m}_\tau$ using (3) starting from $\mathbf{x}$ and color code the result:
   - convergence to a sink $\rightarrow$ assigned color of the sink
   - leaving $D \rightarrow$ color code leaving D
   - exceed maximal number of iterations $\rightarrow$ color code unknown converging behavior
7. Similar to 6. for $\bar{\mathbf{m}}_\tau$.
8. Overlay of the color coding schemes of 6. and 7. gives the complete classification of the asymptotic path line behavior at the time τ.

This algorithm needs some remarks:

To 1. In our application we have chosen not only a single τ but a number of them to show the evolving of the topological sectors over time.

To 2. Since $\mathbf{m}_\tau$ and $\bar{\mathbf{m}}_\tau$ are known to have discontinuities, we sampled them in a rather high resolution and represented them as piecewise bilinear fields.

To 3. To extract the fix points of $\mathbf{m}_\tau$ and $\bar{\mathbf{m}}_\tau$, standard methods for piecewise bilinear fields are applied. However, from the set of extracted fix points we have to remove the ones which are located close to lines of discontinuities of $\mathbf{m}_\tau$ and $\bar{\mathbf{m}}_\tau$. We do so by choosing a small enough neighborhood in which we assume the vector field around the critical point to be continuous. Then we can compute the eigenvalues and eigenvectors of the critical point by sampling inside the neighborhood. With these eigenvalues and eigenvectors, we estimate the vector field inside the neighborhood and compare it with the original vector field. If the estimation error exceeds some threshold, it means there is no continuity inside the neighborhood, and the critical point is invalid.

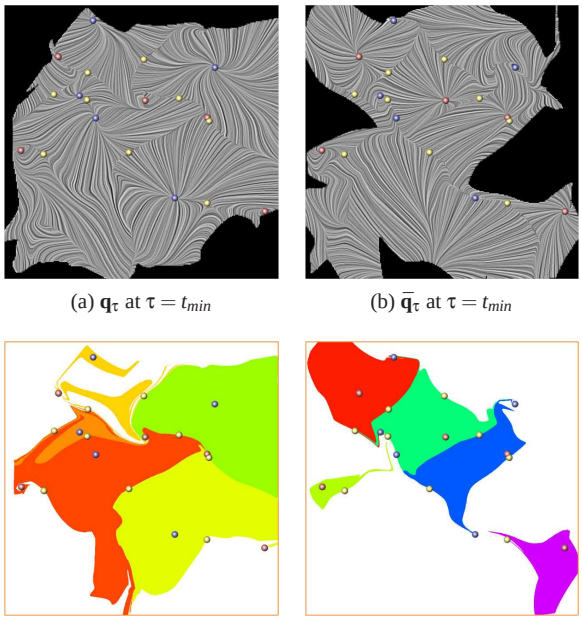

(a) $\mathbf{q}_\tau$ at $\tau = t_{min}$ (b) $\bar{\mathbf{q}}_\tau$ at $\tau = t_{min}$

(c) Basins of $\mathbf{q}_\tau$ at $\tau = t_{min}$ (d) Basins of $\bar{\mathbf{q}}_\tau$ at $\tau = t_{min}$

Figure 7: *The random data set.*

To 4. Inside a cell, the bilinear interpolation of $\mathbf{m}_\tau$ and $\bar{\mathbf{m}}_\tau$ gives the Jacobian of a fix point.

To 5. We used a scheme of random isoluminant colors.

To 6. and 7. The resolution of the sampling for the color coding should not be less than the resolution of $\mathbf{m}_\tau$ and $\bar{\mathbf{m}}_\tau$, in order to deal with the discontinuities of $\mathbf{m}_\tau$ and $\bar{\mathbf{m}}_\tau$.

6. Applications

In this section we apply our technique to a number of test data sets.

Figures 6–7 illustrate our technique at a random vector field. We use random fields as a proof-of-concept because they contain a maximal amount of topological information. The vector field is piecewise trilinear over a $8 \times 8 \times 7$ grid where the time i-th and the $(6-i)$th time slices coincide for $i = 0,..,2$. Figure 6a shows the visualization of $\mathbf{p}$ using LIC planes at three different time slices as well as a number of illuminated stream lines. Figure 7a-7b show the 2D vector fields $\mathbf{q}_\tau$ and $\bar{\mathbf{q}}_\tau$ which correspond to the Poincaré maps $\mathbf{m}_\tau$ and $\bar{\mathbf{m}}_\tau$ for $\tau = t_{min}$. These images have to be interpreted carefully. They clearly show the regions where $\mathbf{q}_\tau$ and $\bar{\mathbf{q}}_\tau$ are undefined (marked black) as well as the locations of the

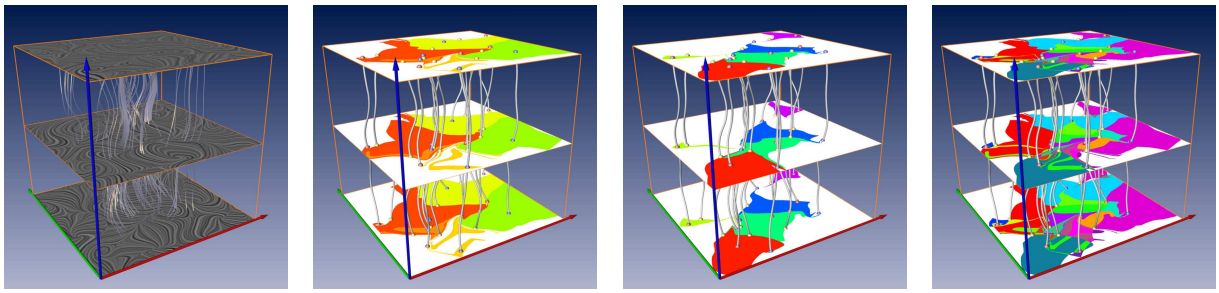

(a) The vector field **p**.

(b) Critical path lines and basins for forward integration.

(c) Critical path lines and basins for backward integration.

(d) Overlayed basins for forward and backward integration.

Figure 6: *The random data set.*

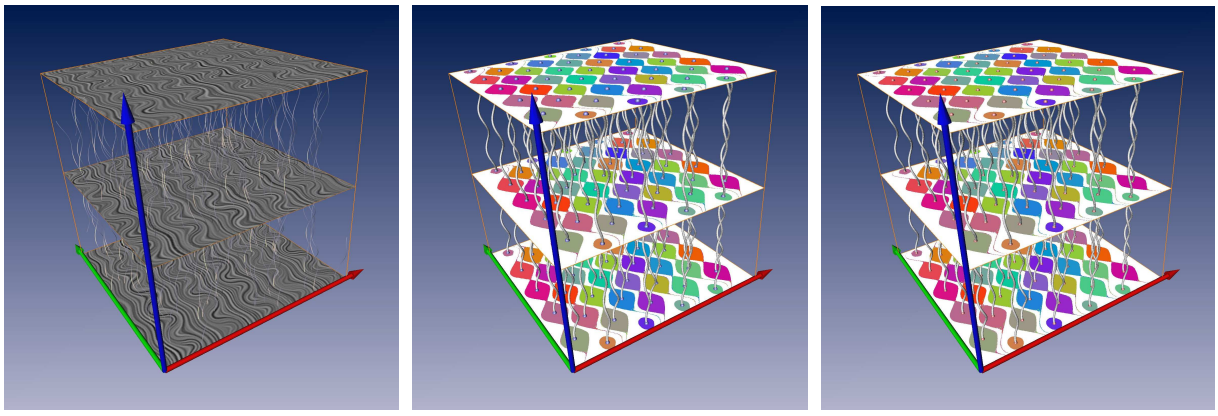

(a) The vector field **p**.

(b) Critical path lines and basins for forward integration.

(c) Critical path lines and basins for backward integration.

Figure 8: *The ABC flow.*

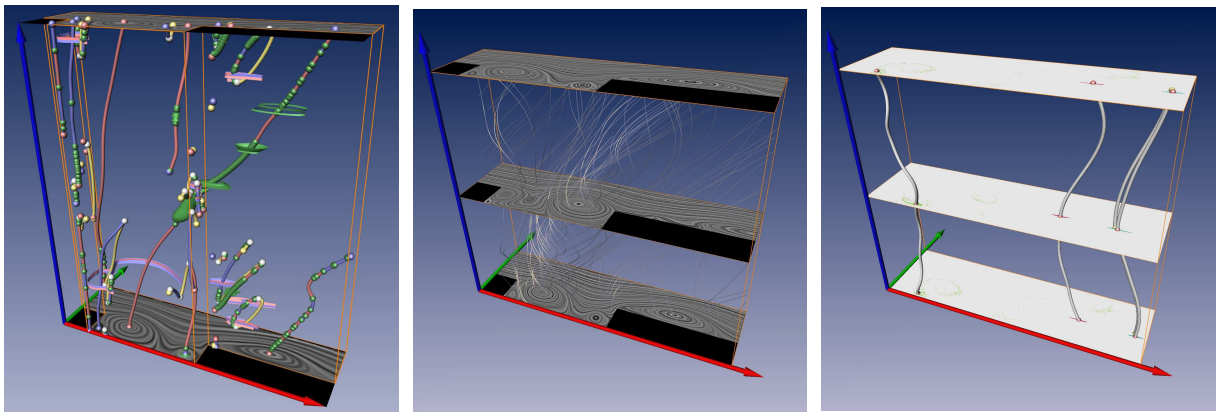

(a) Stream line oriented topology (from [TWHS05])

(b) The vector field **p**.

(c) Critical path lines.

Figure 10: *The cavity data.*

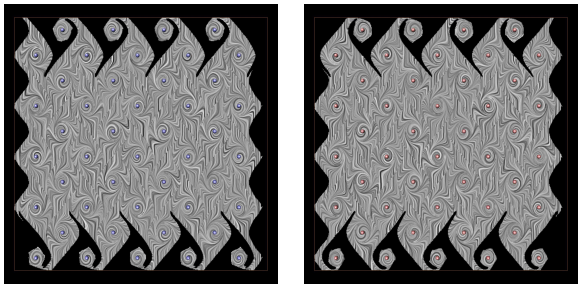

(a) $\mathbf{q}_\tau$ at $\tau = t_{min}$ (b) $\bar{\mathbf{q}}_\tau$ at $\tau = t_{min}$

Figure 9: *The ABC flow.*

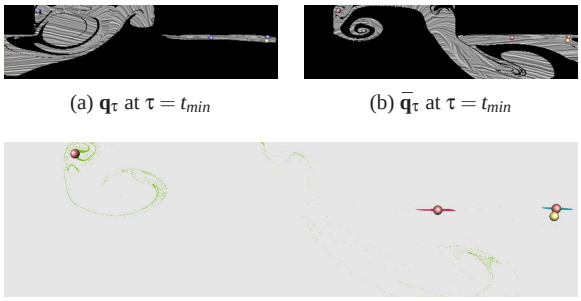

(a) $\mathbf{q}_\tau$ at $\tau = t_{min}$ (b) $\bar{\mathbf{q}}_\tau$ at $\tau = t_{min}$

(c) Critical points and basins of $\bar{\mathbf{q}}_\tau$

Figure 11: *The cavity flow.*

critical points, i.e., the fix points of $\mathbf{m}_\tau$ and $\bar{\mathbf{m}}_\tau$. Also, the LIC images reveal the discontinuities in the Poincaré maps. However, the LIC images also present information about the stream lines of $\mathbf{q}_\tau$ and $\bar{\mathbf{q}}_\tau$. Since only a discrete integration is carried out, stream lines of $\mathbf{q}_\tau$ and $\bar{\mathbf{q}}_\tau$ do not have a physical interpretation.

Figure 6b–6d show the detected 19 critical path lines. 5 of them are sinks in forward integration of $\mathbf{p}$ (marked with blue points), 5 are sinks under backward integration of $\mathbf{p}$ (red points), and 9 are saddles (yellow points). Figure 6b shows the basins of the sinks of $\mathbf{m}_\tau$ for three different times τ. Figure 6b does so for the basins of $\bar{\mathbf{m}}_\tau$. Their overlay is shown in figure 6d, giving the complete classification of the asymptotic behavior of $\mathbf{p}$ starting at one of the selected times τ. The computing time for this data set was 10 minutes for the Poincaré maps in a 1000×1000 resolution, and 1 minute for the basins in a 1000×1000 resolution on a Pentium 4 with 3.40 GHz.

Figures 8–9 visualize parts of the so-called ABC flow which is given by

$$\begin{aligned} u(\mathbf{x}) &= A\sin z + C\cos y, \\ v(\mathbf{x}) &= B\sin x + A\cos z, \\ w(\mathbf{x}) &= C\sin y + B\cos x, \end{aligned} \tag{7}$$

where we set $A = \sqrt{3}$, $B = \sqrt{2}$ and $C = 1$. For our purpose, we considered a cut through the (x,y)-plane and interpret the z-coordinate as the time dimension:

$$\mathbf{p}(\mathbf{x},t) = \begin{pmatrix} \sqrt{3}\sin t + \cos y \\ \sqrt{2}\sin x + \sqrt{3}\cos t \\ 1 \end{pmatrix} \tag{8}$$

The field is periodic in x, y- and t direction with a period of 2π each. We visualize the behavior of the path lines in the domain $[0, 10\pi] \times [0, 10\pi] \times [0, 2\pi]$. Figure 8a shows the LIC plane and the path lines. We detected 45 critical path lines as illustrated in figures 8b and 8c. Figure 9 shows the LIC images of $\mathbf{q}_\tau$ and $\bar{\mathbf{q}}_\tau$: the classification gives that all critical points are weak sinks in $\mathbf{q}_\tau$. The norm of the eigenvalues is only slightly smaller than 1, and the basins are computed using 1000 integration steps. For $\bar{\mathbf{q}}_\tau$, all critical points are weak sinks as well, giving very similarly shaped basins as $\mathbf{q}_\tau$ (figure 8c). Since this contradicts to the property mentioned in section 4.1 (a sink in $\mathbf{q}_\tau$ is a source in $\bar{\mathbf{q}}_\tau$), we conclude that critical points have an unstable center-like behavior: path lines in a certain neighborhood (color coded in figures 8b and 8c) asymptotically remain in this neighborhood without converging/diverging to/from the critical path line. Between these neighborhood regions there are regions where the path lines leave the domain (white areas in figures 8b and 8c)). The computing time for this data set was 10 minutes for the Poincaré maps in a 1000×1000 resolution, and 1 minutes for the basins in a 1000×1000 resolution.

Figures 10–11 show the visualization of a vector field describing the flow at a 2D cavity. This data set was kindly provided by Mo Samimy and Edgar Caraballo (both Ohio State University) [CSJ] as well as Bernd R. Noack (TU Berlin). 1000 time steps have been simulated using the compressible Navier-Stokes equations. The topological behavior of the stream lines of this data set has been analyzed in [TWHS05]. For this data set it turned out that the period appears every 79 time steps. Figure 10b shows $\mathbf{p}$ is one time period by two LIC planes and illuminated stream lines. Figure 10a (from [TWHS05]) shows the stream line oriented topological skeleton. This skeleton has a moderate complexity manifested in a number of moving critical points (represented by the colored lines) and bifurcations. The topological skeleton of our path line oriented topology looks more simple: we detected four critical path lines which are shown in figure 10c. One of them is located inside the cavity, while the others are outside. Three critical path lines are sinks under forward integration and sources under backward integration, the remaining one is a saddle. The total absence of any sinks in forward direction gives the main result of the topological analysis of his data set: every particle (except the ones starting on the critical path lines) is going to leave the cavity after a certain time. Also, it is possible to show the regions from which a backward integration of $\mathbf{p}$ converges to the critical path line: they are shown as colored areas in figure 11c. This figure clearly shows that the basins can have a rather disconnected structure. The computing time for the cavity data set

was 30 minutes for the 3650×1000 Poincaré map, and 5 minutes for the basins in the same resolution. The LIC images of $\mathbf{q}_\tau$ and $\bar{\mathbf{q}}_\tau$ in figures 11a and 11b illustrate this.

7. Conclusions

In this paper we made the following contributions:

- We introduced an approach to analyzing the asymptotic behavior of path lines in periodic time-dependent vector fields.
- We defined, extracted, and classified critical path lines.
- We computed the basins from which the path lines converge to the critical path lines in forward or backward integration.

Our examples show that the path line oriented topology gives significantly different topological information than the stream line oriented one. The main disadvantage of our approach is that it is limited to periodic vector fields only. In fact, we do not see a way to straightforwardly extend it to non-periodic vector fields. However, we think that due to the number of periodic vector fields obtained from time-dependent numerical flow simulations, this class of vector field data deserves the special consideration.

Acknowledgment

We thank Bernd R. Noack for the fruitful discussions and the supply of the cavity data set which was kindly provided by Mo Samimy and Edgar Caraballo.

All visualizations in this paper have been created using AMIRA – a system for advanced 3D visualization and volume modeling [SWH05] (see `http://amira.zib.de/`).

References

[BMH01] BISCHI G.-I., MROZ L., HAUSER H.: Studying basin bifurcations in nonlinear triopoly games by using 3d visualization. *Journal Nonlinear Analysis 47*, 8 (2001), 5325–5341.

[CSJ] CARABALLO E., SAMIMY M., J D.: Low dimensional modeling of flow for closed-loop flow control. AIAA Paper 2003-0059.

[dLvL99a] DE LEEUW W., VAN LIERE R.: Collapsing flow topology using area metrics. In *Proc. IEEE Visualization '99* (1999), pp. 149–354.

[dLvL99b] DE LEEUW W., VAN LIERE R.: Visualization of global flow structures using multiple levels of topology. In *Data Visualization 1999. Proc. VisSym 99* (1999), pp. 45–52.

[GLL91] GLOBUS A., LEVIT C., LASINSKI T.: A tool for visualizing the topology of three-dimensional vector fields. In *Proc. IEEE Visualization '91* (1991), pp. 33–40.

[GTS04] GARTH C., TRICOCHE X., SCHEUERMANN G.: Tracking of vector field singularities in unstructured 3D time-dependent datasets. In *Proc. IEEE Visualization 2004* (2004), pp. 329–336.

[HH89] HELMAN J., HESSELINK L.: Representation and display of vector field topology in fluid flow data sets. *IEEE Computer 22*, 8 (August 1989), 27–36.

[HMBG01] HAUSER H., MROZ L., BISCHI G.-I., GRÖLLER E.: Two-level volume rendering. *IEEE Transactions on Computer Graphics 7*, 3 (2001), 242–252.

[LDG98] LÖFFELMANN H., DOLEISCH H., GRÖLLER E.: Visualizing dynamical systems near critical points. In *Spring Conference on Computer Graphics and its Applications* (Budmerice, Slovakia, 1998), pp. 175–184.

[LKG98] LÖFFELMANN H., KUČERA T., GRÖLLER E.: Visualizing poincaré maps together with the underlying flow. In *Proc. VisMath '97* (1998), pp. 315–328.

[Löf98] LÖFFELMANN H.: *Visualizing Local Properties and Characteristic Structures of Dynamical Systems*. PhD thesis, Vienna Univserity of Technology, 1998.

[LRR00] LODHA S., RENTERIA J., ROSKIN K.: Topology preserving compression of 2D vector fields. In *Proc. IEEE Visualization 2000* (2000), pp. 343–350.

[MBS*04] MAHROUS K., BENNETT J., SCHEUERMANN G., HAMANN B., JOY K.: Topological segmentation in three-dimensional vector fields. *IEEE Transactions on Visualization and Computer Graphics 10*, 2 (2004), 198–205.

[SKMR98] SCHEUERMANN G., KRÜGER H., MENZEL M., ROCKWOOD A.: Visualizing non-linear vector field topology. *IEEE Transactions on Visualization and Computer Graphics 4*, 2 (1998), 109–116.

[SWH05] STALLING D., WESTERHOFF M., HEGE H.-C.: Amira: A highly interactive system for visual data analysis. *The Visualization Handbook* (2005), 749–767.

[The02] THEISEL H.: Designing 2D vector fields of arbitrary topology. *Computer Graphics Forum (Eurographics 2002) 21*, 3 (2002), 595–604.

[TRS03] THEISEL H., RÖSSL C., SEIDEL H.-P.: Compression of 2D vector fields under guaranteed topology preservation. *Computer Graphics Forum (Eurographics 2003) 22*, 3 (2003), 333–342.

[TS03] THEISEL H., SEIDEL H.-P.: Feature flow fields. In *Data Visualization 2003. Proc. VisSym 03* (2003), pp. 141–148.

[TSH00] TRICOCHE X., SCHEUERMANN G., HAGEN H.: A topology simplification method for 2D vector fields. In *Proc. IEEE Visualization 2000* (2000), pp. 359–366.

[TSH01] TRICOCHE X., SCHEUERMANN G., HAGEN H.: Continuous topology simplification of planar vector fields. In *Proc. Visualization 01* (2001), pp. 159 – 166.

[Tso92] TSONIS A.: *Chaos - From Theory to Applications*. Plenum Press, 1992.

[TSW*05] THEISEL H., SAHNER J., WEINKAUF T., HEGE H.-C., SEIDEL H.-P.: Extraction of parallel vector surfaces in 3d time-dependent fields and application to vortex core line tracking. In *Proc. IEEE Visualization 2005* (2005), pp. 631–638.

[TWHS03] THEISEL H., WEINKAUF T., HEGE H.-C., SEIDEL H.-P.: Saddle connectors - an approach to visualizing the topological skeleton of complex 3D vector fields. In *Proc. IEEE Visualization 2003* (2003), pp. 225–232.

[TWHS05] THEISEL H., WEINKAUF T., HEGE H.-C., SEIDEL H.-P.: Topological methods for 2D time-dependent vector fields based on stream lines and path lines. *IEEE Transactions on Visualization and Computer Graphics 11*, 4 (2005), 383–394.

[TWSH02] TRICOCHE X., WISCHGOLL T., SCHEUERMANN G., HAGEN H.: Topology tracking for the visualization of time-dependent two-dimensional flows. *Computers & Graphics 26* (2002), 249–257.

[WJE01] WESTERMANN R., JOHNSON C., ERTL T.: Topology-preserving smoothing of vector fields. *IEEE Transactions on Visualization and Computer Graphics 7*, 3 (2001), 222–229.

[WS01] WISCHGOLL T., SCHEUERMANN G.: Detection and visualization of closed streamlines in planar flows. *IEEE Transactions on Visualization and Computer Graphics 7*, 2 (2001), 165–172.

[WSH01] WISCHGOLL T., SCHEUERMANN G., HAGEN H.: Tracking closed stream lines in time-dependent planar flows. In *Proc. Vision, Modeling and Visualization 2001* (2001), pp. 447–454.

[WTHS04a] WEINKAUF T., THEISEL H., HEGE H.-C., SEIDEL H.-P.: Boundary switch connectors for topological visualization of complex 3D vector fields. In *Data Visualization 2004. Proc. VisSym 04* (2004), pp. 183–192.

[WTHS04b] WEINKAUF T., THEISEL H., HEGE H.-C., SEIDEL H.-P.: Topological construction and visualization of higher order 3D vector fields. *Computer Graphics Forum (Eurographics 2004) 23*, 3 (2004), 469–478.

[WTS*05] WEINKAUF T., THEISEL H., SHI K., HEGE H.-C., SEIDEL H.-P.: Topological simplification of 3d vector fields by extracting higher order critical points. In *Proc. IEEE Visualization 2005* (2005), pp. 559–566.